ing), we do not believe that this is in any way contradictory because we have previously demonstrated that the structure of the monolayers depends on the chain length; in the limit of small chain lengths, the structure should be dominated by the interface, which would be expected to result in a simple $\sqrt{3} \times \sqrt{3}R30°$ structure. Furthermore, a recent theoretical calculation has found that the adsorption process [that is, a thiol forming a thiolate on Au(111) and releasing hydrogen in the form of H_2] may be endothermic by a few kilocalories per mole (*7*) and may consequently argue against the thiolate structure.

Recent STM results [which find a C(4 × 2) unit cell] find an apparent height modulation of symmetry-inequivalent molecules that are hexagonally packed lateral to the surface (*10*). This is fully consistent with our derived structure and may be caused by both the inequivalent sulfur bonding sites as well as the different twists of the hydrocarbon chains about the chain axis. A detailed comparison of the x-ray and STM results may provide a unique opportunity to understand the tunneling mechanism in these films. A height modulation of the hydrocarbon chains may also explain the sensitivity of He atom diffraction to the C(4 × 2) structure (*17*), even though He atom diffraction does not directly probe the monolayer-substrate interface. Finally, we expect that nature of the bonding to the substrate may explain the discrepancy between the greater thermal stability and lack of rotator phases in our previously observed (*15*) experimental phase behavior, as compared to both the predicted monolayer (*8*) and the known bulk *n*-alkane phase behaviors (*21*).

These results imply an entirely new context in which to view the self-assembly of these materials. In particular, previous results on the structure, defects, molecular diffusion, as well as the self-assembly process itself may need to be reinterpreted. The presence of a gauche defect at the S–C bond is at first surprising. Yet, because the energy cost of an isolated gauche defect is comparable to thermal energies (*22*), there will be a significant density of gauche bonds for an isolated molecule. Clearly, the self-assembly process includes internal conformational changes to form a dense layer consisting of extended hydrocarbon chains, and it is not difficult to imagine that gauche defects that reduce the steric or bonding constraints in these complex systems may be readily accommodated.

The resulting difference between the head group and hydrocarbon chain spacings provides a simple illustration of the structural versatility in these systems. This highlights the importance of both conformational degrees of freedom and the impact of the interface on the film structure, which may result in both novel structures and growth modes. It also raises the possibility of using internal molecular degrees of freedom (for example, conformations) within supramolecular assemblies and in the epitaxy of wide classes of "soft-soft" and "soft-hard" growth systems [such as organic quantum well structures (*23*) and the bio-mineral interface (*24*), respectively] as a means to reduce or eliminate the need for lattice matching in these systems.

REFERENCES AND NOTES

1. L. H. Dubois and R. G. Nuzzo, *Annu. Rev. Phys. Chem.* **43**, 437 (1992).
2. J. D. Swalen *et al.*, *Langmuir* **3**, 932 (1987).
3. A. Ulman, *An Introduction to Ultrathin Organic Films* (Academic Press, San Diego, CA, 1991).
4. N. Camillone III, C. E. D. Chidsey, G.-Y. Liu, T. M. Putvinski, G. Scoles, *J. Chem. Phys.* **94**, 8493 (1991).
5. L. H. Dubois, B. R. Zegarski, R. G. Nuzzo, *ibid.* **98**, 678 (1993).
6. R. G. Nuzzo, L. H. Dubois, D. L. Allara, *J. Am. Chem. Soc.* **112**, 558 (1990).
7. H. Sellers, *Surf. Sci.* **294**, 99 (1993).
8. J. Hautman and M. L. Klein, *J. Chem. Phys.* **93**, 7483 (1990).
9. C. D. Bain *et al.*, *J. Am. Chem. Soc.* **111**, 321 (1989).
10. G. E. Poirier and M. J. Tarlov, *Langmuir* **10**, 2853 (1994).
11. C. D. Bain, H. A. Biebuyck, G. M. Whitesides, *ibid.* **5**, 723 (1989).
12. R. G. Nuzzo, B. R. Zegarski, L. H. Dubois, *J. Am. Chem. Soc.* **109**, 733 (1987).
13. H. A. Biebuyk and G. M. Whitesides, *Langmuir* **9**, 1766 (1993).
14. P. Fenter *et al.*, unpublished results.
15. P. Fenter, P. Eisenberger, K. S. Liang, *Phys. Rev. Lett.* **70**, 2447 (1993).
16. N. Camillone III *et al.*, *J. Chem. Phys.* **99**, 744 (1993).
17. N. Camillone III, C. E. D. Chidsey, G.-Y. Liu, G. Scoles, *ibid.* **98**, 3503 (1993).
18. B. Beagley and K. T. McAloon, *Trans. Faraday Soc.* **67**, 3216 (1971).
19. X. Gao, Y. Zhang, M. J. Weaver, *J. Phys. Chem.* **96**, 4156 (1992).
20. R. G. Nuzzo, F. A. Fusco, D. L. Allara, *J. Am. Chem. Soc.* **109**, 2358 (1987).
21. D. M. Small, *The Physical Chemistry of Lipids: From Alkanes to Phospholipids* (Plenum, New York, 1986).
22. J. F. Nagle, *Faraday Discuss. Chem. Soc.* **81**, 151 (1986).
23. F. F. So, S. R. Forrest, Y. Q. Shi, W. H. Steier, *Appl. Phys. Lett.* **56**, 674 (1990).
24. S. Mann *et al.*, *Science* **261**, 1286 (1993).

25. We acknowledge the close interaction with J. Li, N. Camillone III, G.-Y. Liu, T. A. Ramanarayanan, C. E. D. Chidsey, G. Scoles, and K. Liang throughout these studies. This work is supported by National Science Foundation award DMR-9311871 and was performed at the NSLS, which is supported by Department of Energy contract DE-AC0276CH-00016.

27 June 1994; accepted 7 September 1994

Growth and Sintering of Fullerene Nanotubes

D. T. Colbert, J. Zhang, S. M. McClure, P. Nikolaev, Z. Chen,
J. H. Hafner, D. W. Owens, P. G. Kotula, C. B. Carter,
J. H. Weaver, A. G. Rinzler, R. E. Smalley*

Carbon nanotubes produced in arcs have been found to have the form of multiwalled fullerenes, at least over short lengths. Sintering of the tubes to each other is the predominant source of defects that limit the utility of these otherwise perfect fullerene structures. The use of a water-cooled copper cathode minimized such defects, permitting nanotubes longer than 40 micrometers to be attached to macroscopic electrodes and extracted from the bulk deposit. A detailed mechanism that features the high electric field at (and field-emission from) open nanotube tips exposed to the arc plasma, and consequent positive feedback effects from the neutral gas and plasma, is proposed for tube growth in such arcs.

In 1991 Iijima (*1*) discovered that micrometer lengths of a multiwalled, somewhat imperfect version of tubular fullerenes were present in the same sort of carbon arc apparatus already used to make C_{60} and other small, spheroidal fullerenes. Much progress has been made in increasing the yield of such nanotubes (*2*) and in purification (*3, 4*), but substantial quantities of carbon nanotubes are still not generally available with a perfect graphene structure over sufficient lengths that they truly deserve the term fullerene tubes (*5*) or fibers. The studies reported below show that sintering of adjacent nanotubes to each other due to the high-temperature conditions of growth is the principal cause of defects in nanotubes produced in arcs. We have uncovered striking new clues of why nanotubes grow in such abundance in such arcs, and present a detailed mechanistic model for this growth.

Following on the initial work by Ebbesen and Ajayan (*2*), our first study of carbon

---

D. T. Colbert, J. Zhang, S. M. McClure, P. Nikolaev, Z. Chen, J. H. Hafner, A. G. Rinzler, R. E. Smalley, Rice Quantum Institute and the Departments of Chemistry and Physics, M.S. 100, Rice University, P.O. Box 1892, Houston, TX 77251, USA.

D. W. Owens, P. G. Kotula, C. B. Carter, J. H. Weaver, Electronic Materials Group, Department of Chemical Engineering and Materials Science, University of Minnesota, 421 Washington Avenue, S.E., Minneapolis, MN 55455, USA.

---

*To whom correspondence should be addressed.

nanotube production used the carbon arc apparatus developed earlier in this group for the generation of fullerenes (*6*) with the simple change of operating at a somewhat higher helium buffer gas pressure (500 torr). When operating with 6-mm diameter graphite electrodes, we observed a nanotube-rich deposit form on the cathode just as reported by previous workers (*1*, *2*). However, operation with 12.5-mm-diameter rods produced a hard, gray-white core in the cylindrical boule deposit, whereas with the 6-mm rods the core was flat-black, easily broken apart, and very rich in nanotubes.

Wang *et al.* (*7*) reported similar results and argued that this central core was too cool during the operation of the arc to permit nanotubes to grow. However, we suspected the reverse was actually the case: The core was getting too hot, with the result that the nanotube material there was sintering together. This tube tube sintering might be similar to the fullerene-fullerene coalescence process found to occur readily at high temperatures in a variety of experiments (*8–10*). At sufficiently high temperatures, the sintering of the tubes could progress to the extent that the width and length of the average graphene sheet bridging across large groups of sintered tubes would be larger than the wavelength of visible light, and the reflectivity of the material would resemble that of graphite—more gray than black.

Replacing the 50-mm-long, 12.5-mm-diameter graphite cathode with one made of copper showed that overheating was indeed the problem. Although both were attached to water-cooled electrode mounts, the difference in thermal conductivity was sufficient to make a vivid difference in the nature of the carbon boule formed. The cooler-running copper cathode resulted in a uniform flat-black boule with no gray-white central core. Experience in manipulating these nanotube-rich, flat black deposits has shown they are composed of parallel 50-μm diameter columns aligned along the central axis of the electrodes (*11–13*), that the deposit is readily cleaved parallel to these columns, and that individual columns are easily picked out of the boule with tweezers. The core of the boule grown on the water-cooled copper cathode was still somewhat harder, more difficult to cleave or pick out individual columns than the outer annular region, indicating that although the better cooling had made a big improvement, tube tube sintering had not been eliminated entirely.

A scanning electron microscope (SEM) image of a section of one of these 50-μm columns (Fig. 1) shows that the column appears to be composed of parallel nanotubes, most of which appear to be sintered to other tubes in bundles, and that there is a large amount of intervening nanoscale debris. Most of this debris is of the right size to be what we believe are broken bits of sintered nanotube. Sintering of the nanotubes causes them to weaken structurally because the graphene sheets must expose open edges as they bridge from one tube to the next. These open edges serve as localization sites for mechanical stress. As the tubes sinter, they pack much more closely. Lateral forces build up from the sintering (along their lengths) of many tubes bound together in different groupings, then result in extensive breakage and embrittlement.

In order to further enhance cooling and to maintain optimum arcing conditions, the apparatus shown schematically in Fig. 2 was constructed. The (top) anode and (bottom) copper cathode mounts are rigorously coaxial and equipped with computer-controlled stepping motors for rotation and translation about the vertical axis. The region around the arc was completely enclosed in water-cooled copper surfaces (*14*). Graphite electrodes as large as 19-mm diameter were used to produce high-quality nanotube boules. When short lengths (<2.5 cm) of graphite rod were attached to the water-cooled cathode mount, conduction down the length of this graphite electrode was sufficient to prevent formation of the gray-white core. The best production of nanotube material coincided with a remarkably stable operating condition of the arc where the cathode-anode gap was 1 to 2 mm, the plasma of the arc appeared by eye to uniformly extend over the entire electrode surface, and very little fluctuation was seen either as flashes in the brightness of the arc, the anode-cathode voltage drop, or the vertical translational motion of the electrodes as the computer feedback circuit worked to control the voltage. With 12.5-mm-diameter electrodes, this stable operation could be attained in the range of 17 to 20 V and 110 to 130 A; with 19-mm electrodes these stable voltage conditions were 17 to 20 V but 250 to 300 A. In both cases, 90 ± 5% of the carbon that evaporated from the anode deposited directly on the cathode. The process is very much like zone refining, except the plasma takes the place of the molten zone. As explained below, we suspect this extremely steady behavior of the arc is not a coincidence. It is caused by the cathode being covered by tens of thousands of parallel columns, each of which is composed of millions of parallel nanotubes. Each of these nanotubes acts as an intense field-emitter of electrons into the plasma of the arc.

When operated under such stable arcing conditions, the boules of carbon cathode deposit were uniformly flat black across their diameter, except for a thin (<1 mm) outer gray skin on the side. As noted above, these boules contained parallel columns $\sim$50 μm in diameter, and cross sections of the boule parallel to the cylinder axis usually showed the columns to extend with remarkable straightness and clear delineation all the way from the bottom (start) of

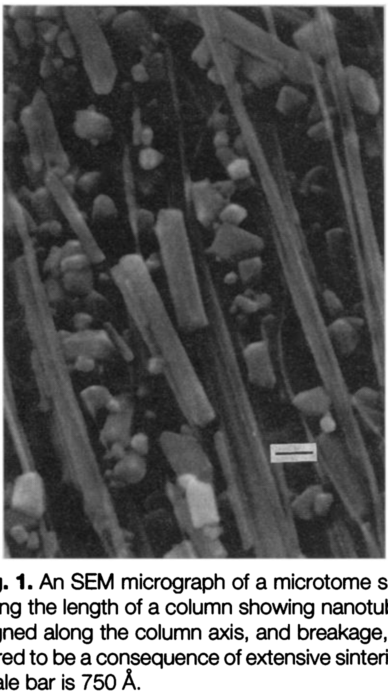

Fig. 1. An SEM micrograph of a microtome slice along the length of a column showing nanotubes aligned along the column axis, and breakage, inferred to be a consequence of extensive sintering; scale bar is 750 Å.

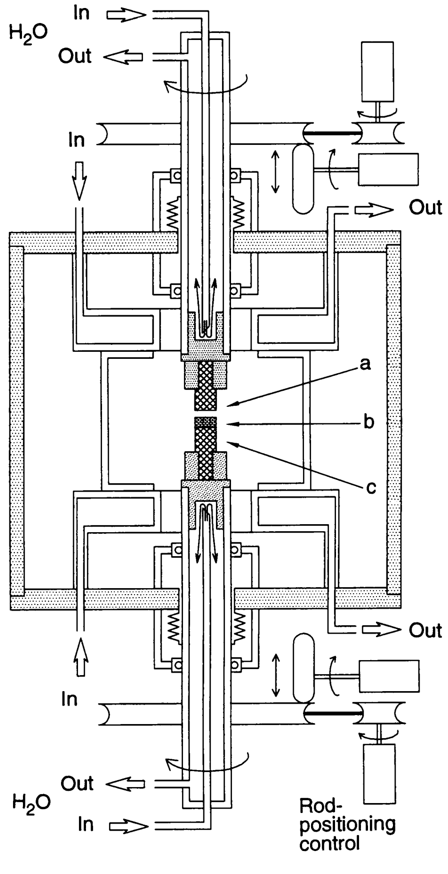

Fig. 2. Schematic of the arc apparatus for generating carbon nanotubes; a, graphite anode; b, deposit; and c, graphite cathode.

the deposit to the top. The spacing and diameter of these columns varied somewhat across the radius of the boule, but often they formed a strikingly regular pattern. A low-resolution SEM view of the top of such a region of a boule deposit on 19-mm electrodes is shown in Fig. 3. The tops of the columns are seen here end-on as 50-μm-diameter circles, which we refer to as zone 1, spaced ~50 μm apart on a roughly hexagonal lattice, whose intervening material we call zone 2. Oblique views of the top surface of the boule immediately after it was removed from the arc apparatus showed the tops of the columns to be hemispherical. Higher resolution SEM views of the column tops and the intervening regions showed the entire surface to consist of vast numbers of nanotubes and nanoparticles with no evident order. Generally this top surface morphology was best revealed by blowing off the fine carbon dust from the surface.

We oxidatively etched the boule following Ebbesen *et al.* (*4*) to purify the nanotube material (*15*), by simply heating a 19-mm boule grown under optimized conditions in a stream of air at 650°C and 1 atm of pressure for 30 min. This etch burned away the columns of zone 1, leaving ~50-μm-diameter holes though the boule surrounded by swirls of nanotubes in zone 2 (Fig. 4A). This differential etching effect is even more clearly seen in Fig. 4B, which is an SEM image of the cleaved side of a boule, showing the side and top after the 650°C bake. Here the boule has been revealed to be somewhat like a wasp nest, with empty holes where the columns of zone 1 had been. A higher resolution SEM image of the zone 2 material surrounding the vertical holes (Fig. 4C) shows that it consists entirely of a tangle of nanotubes, but with their tube axes mostly perpendicular to the viewing axis (which here was parallel to the central axis of the boule). Note also that the individual nanotubes often run together with some other tubes for some distance, and then separate again. These frequent "comings and goings" are characteristic of these zone 2 deposits as revealed by the oxidative etch.

The nanotubes present in zone 2 are generally so tangled with one another that it has not been possible to determine their length by measuring in any microscopic view. The typical procedure used to isolate individual nanotubes for study [since the original work of Iijima (*1*)] has been to sonicate a slurry of the nanotube material in a liquid such as methanol, and then sample a small amount of the suspension (*3*). We find that this procedure samples primarily just short bits broken off from the main tangle, which only becomes more tangled as grinding and sonication is continued. Instead, we have had some success with gluing one side of the tip of a hypodermic needle to the top of an oxidatively etched zone 2 deposit and then "pulling" out a small group of nanotube fibers from the tangled mass. Figure 4D shows an SEM view of one such experiment. By using electrically conductive "silver paint" on the stainless steel hypodermic needles or standard tin-lead solder on sharpened copper wires, we have verified that these mounted nanotubes are well connected electrically by monitoring field emission from their tips at levels of up to and at times exceeding 10^{-7} A per tube at bias voltages of less than −200 V, under medium high vacuum conditions (10^{-7} to 10^{-6} torr). We have obtained individual nanotubes produced in zone 2 in this fashion as long as 40 μm. We find the nanotubes drawn out of the zone 2 region by this technique are often in bundles of 10 or more, but these bundles almost always thin down to fewer nanotubes with increasing distance from the point of attachment, until at the end there is generally just a single tube.

The strikingly regular morphology of zones 1 and 2 of the carbon deposit on the cathode is, to our knowledge, completely unprecedented in arcs or discharges of any

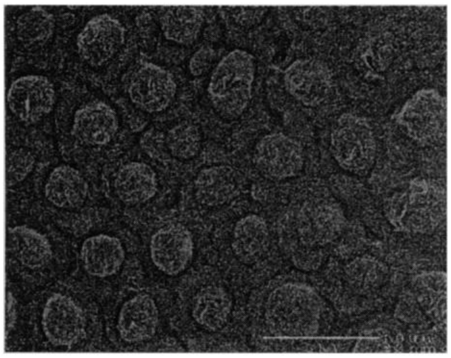

Fig. 3. Top view (SEM) of a section of the carbon deposit (boule) produced in the arc apparatus of Fig. 2, showing regular triangular arrangement of zone 1 column tops and intervening zone 2 regions; scale bar is 100 μm.

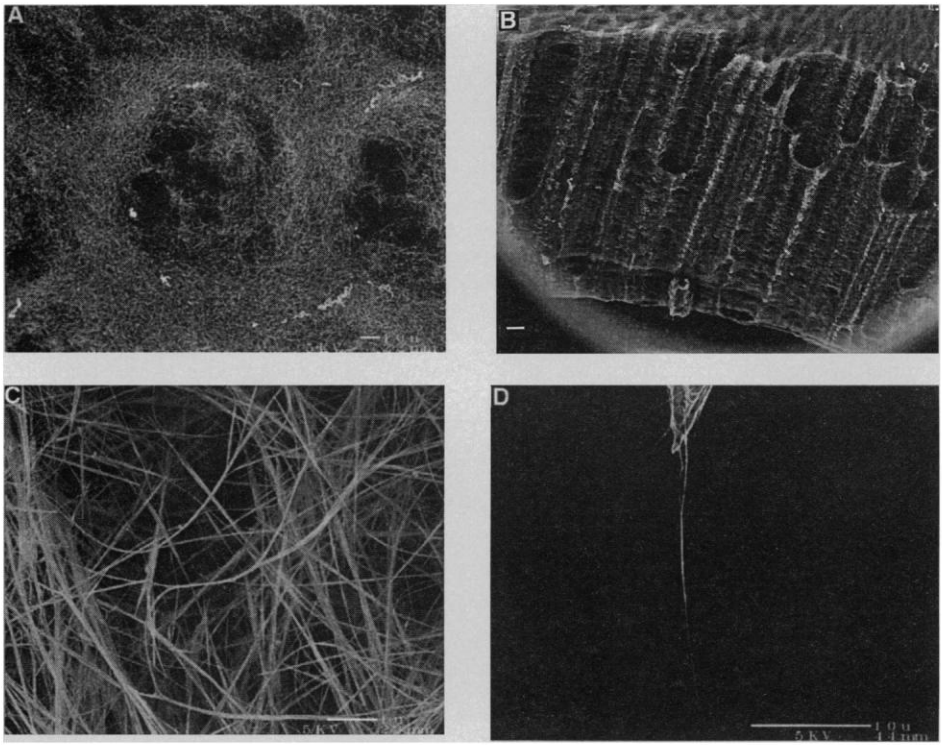

Fig. 4. (**A**) Magnified top view of the same region as Fig. 3 after oxidative etching at 650°C in air for 30 min; scale bar is 10 μm. Note the columns of Fig. 3 have now etched away completely, leaving tangles of pure nanotubes from the intervening zone 2 deposit. (**B**) Side view of the oxidatively etched nanotube boule, showing the "wasp's nest" of columns that have preferentially etched away; scale bar is 100 μm. Only zone 2 nanotubes remain. Nanotubes originally present in the columns of zone 1 have oxidized preferentially because their strong axial alignment resulted in extensive sintering, which in turn introduced defects and breakage leading to rapid oxidative etching. (**C**) Detail of nanotubes in zone 2 after oxidative etch. Note the nearly total lack of material other than nanotubes; scale bar is 1 μm. Also, if one follows a single nanotube, one sees it come and go with other nanotubes. This morphology suggests that zone 2 nanotubes are never aligned at any point in their growth. (**D**) An SEM view of needle-mounted fullerene nanotubes harvested from zone 2. These tubes, which are almost long and perfect enough to deserve the term "fullerene fibers," are attached with good electrical continuity to the tip of a stainless steel hypodermic needle with "silver paint." They were pulled out of an oxidatively purified zone 2 deposit of nanotubes similar to that shown in (A) to (C). The tube shown here extends 24 μm beyond its point of attachment on the needle.

kind. Something unusual must be occurring in the physics of the arc to produce these effects. Aside from some conjectures about the relevance of electric fields (*12*, *16*) and the paths of current flow in the arc (*11*, *17*), no detailed mechanism has yet been advanced for nanotube growth. The new clues provided by the zone 1 and zone 2 morphologies lead us to propose the model shown schematically in Fig. 5. The key feature in this new model is the effect of zone 1 on operation of the arc. Here the open tips of millions of parallel nanotubes act as highly effective field emitters—so effective that this field emission becomes the dominant mechanism for electron injection into the plasma of the arc. In response, the carbon ion density and current flow in the plasma become concentrated in regions above these zone 1 columns. This plasma structure in turn enhances and sustains the growth of the zone 1 structure on the cathode.

We assume in this model, as argued previously (*16*), that carbon nanotubes grow rapidly only when their tips are open, and that this open condition can only be sustained at the 3000°C temperature of the cathode surface when a high electric field is present that inhibits their closure (*18*). In our model, this condition is attained at the top of the zone 1 columns because the high carbon ion current flowing to these columns produces a thin "cathode fall" layer (*19*) where the potential drops $\sim$10 V over a distance of less than 0.5 μm. The high electric field in this layer is concentrated further at the tips of the nanotubes, reaching values near 1 V/Å. This extremely high field keeps the nanotube tips open and thereby enhances not only the electron emission from their tips but also serves to attract the positive carbon ions that in this region provide the dominant feedstock for nanotube growth. The enhanced flux of C^+ in the region of the columns favors the growth of nanotubes parallel to each other, spaced as closely as possible so as to provide the largest effective field emission current density, but spaced by at least one tube diameter (as shown in the top right inset of Fig. 5) so as not to "shadow" the tip of any nanotube in the electric field of its neighbors.

Elastic collisions with the helium buffer gas preserve the energy of the field-emitted electrons while forcing them to diffuse over a distance of several column diameters ($\sim$100 μm) above zone 1, leading to a high degree of ionization of carbon (*20*) in this region. Because this distance is many times the He-C^+ mean free path ($\sim$2 μm), the downward-directed carbon ion current then transfers momentum, through collisions, to the helium buffer gas, producing a "wind" (*21*) in the neutral gas directed at the tops of the columns.

In our model, this wind is responsible for formation of zone 2. Because the helium wind cannot react with the carbon at the top of the column, it must sweep to the side. This effect creates an inert boundary layer that increasingly inhibits the growth of nanotubes on the periphery of zone 1 by deflecting the C^+ feedstock. Because the local C^+ current is created primarily from field emission by the nanotubes themselves, and because nanotubes that cannot grow fast enough to keep up with their neighbors will have their tips "shadowed" and will therefore close and stop growing, the termination of parallel nanotube growth at the edge of zone 1 is quite abrupt. The exhaust gas from this helium flow over the column tops of zone 1 must then recycle back up into the plasma, being driven by a slight pressure differential. This process occurs over zone 2. If the pressure differential is small, the flow velocities will be similar and the net area of zone 2 will be only slightly larger than zone 1. The result for an overall flat electrode gap is a hexagonal lattice of structures where the zone 1 columns are spaced by slightly less than their diameters. The pattern is similar to that of Bénard convection cells (*22*) in fluids, except that here the downward flow is driven by momentum transfer from a directed ion current, rather than the thermally induced buoyancy effects in true convection cells, and in our model it is a slight pressure gradient that drives the return flow (*23*).

The pressure differential that drives the unreactive helium out past the column also sweeps with it carbon feedstock into zone 2. Neutral carbon evaporated from zone 1 nanotubes supply a large portion of this feedstock. The evaporation rate can be estimated from the boule growth rate, which under our optimized conditions is 3×10^{-4} cm s^{-1}. For an average boule density of 1 g cm^{-3}, the bulk growth rate would be then 1.5×10^{19} atoms per square centimeter per second. However, this is only 10% of the carbon ion current density (*24*) going to the tops of the columns of zone 1. The majority of carbon ions and neutrals that strike the columns of zone 1 must therefore evaporate as neutrals. This high evaporation rate explains why perfect nanotubes are initially (prior to sintering) so dominant in the cathode deposit: Other less stable structures evaporate too quickly to survive.

The carbon structures that grow successfully in zone 2 are also dominated by fullerene nanotubes, except that now there is no reason for them to be parallel. Nanotubes can grow here because the positive carbon ion density in this region is still high enough to produce an abrupt 10-V potential drop at the tips of any nanotube on the surface over a distance of less than 100 nm (the Debye length at 10^{16} cm^{-3}). This will generate an electric field of nearly 1 V/Å at the open tips of the nanotubes as long as they are on the top of the pile of other nanotubes in this region and each tip is further than 50 to 100 nm from any other tube. Inspection of the tangled pile of zone 2 nanotubes shown in Fig. 4C shows that this spacing requirement is readily met. As in zone 1, the high temperature of the cathode surface ensures that only the most stable, most rapidly growing structures can compete with evaporation and survive.

This model explains nanotube growth in dc arcs as a subtle interaction between field-emitting structures on the cathode and the plasma itself. Like convection cells in fluid media (*22*), and many other examples in physics, chemistry, and biology, it is a case of elaborate, symmetric structures self-organiz-

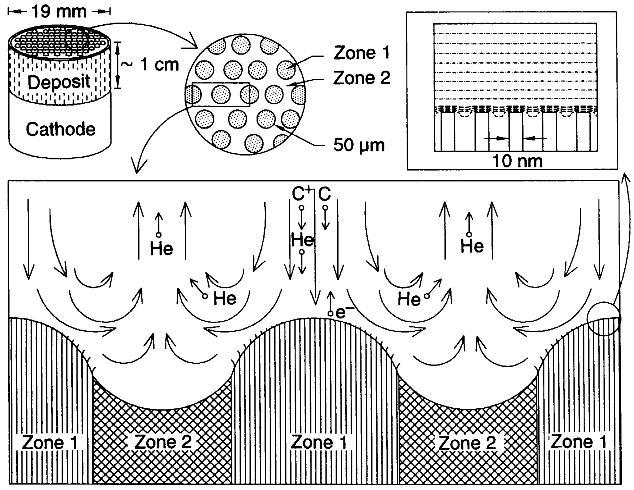

Fig. 5. Schematic of carbon nanotube growth model in a dc arc. The small panels on the upper left and center show schemata of the column structure, whereas the main panel shows a schematic of the helium wind over a column of zone 1 nanotubes. The wind is created by collisions of carbon ions with helium as the ions are drawn by the electric field toward the cathode. Zone 2 exists because of the need for a return path. Field emission of electrons from the tips of the nanotubes in the columns of zone 1 produces a high degree of carbon ionization above the columns. These C^+ ions are then drawn to the tops of the columns, providing the principal feedstock for their growth. The small panel on the upper right show calculated equipotential lines in a portion of the cathode layer above individual open-tipped nanotubes, which are at 0 V. The dot-dashed lines correspond to potential values from 0.2 to 0.4 V, spaced by 0.2 V, and the dashed curves to potentials of 0.2, 0.15, 0.1, and 0.05 V.

ing in a nonlinear complex system driven far from equilibrium (*25*). In this case, the model suggests that essentially all of the carbon condensing on the cathode is initially in the form of perfect fullerene fibers, purified in the "zone refining" of the arc. Although these nanofibers are highly stable in isolation on the nanometer scale, when touching each other on the macroscale they are, unfortunately, only metastable. The same fire that gives birth to them in the arc also leads to their destruction by sintering (*26*). Still, much can be made from those nanotubes that survive (imperfect as they may be) in the ashes of zone 1 and in the tangles of zone 2.

REFERENCES AND NOTES

1. S. Iijima, *Nature* **354**, 56 (1991).
2. T. W. Ebbesen and P. M. Ajayan, *ibid.* **358**, 220 (1992).
3. K. Tanaka *et al.*, *Chem. Phys. Lett.* **223**, 65 (1994).
4. T. W. Ebbesen, P. M. Ajayan, H. Hiura, K. Tanigaki, *Nature* **367**, 519 (1994).
5. O. Zhou *et al.*, *Science* **263**, 1744 (1994).
6. R. E. Haufler *et al.*, *Mater. Res. Soc. Symp. Proc.* **206**, 627 (1991).
7. X. K. Wang, X. W. Lin, V. P. Dravid, J. B. Ketterson, R. P. H. Chang, *Appl. Phys. Lett.* **62**, 1881 (1993).
8. Y. Chai *et al.*, *J. Phys. Chem.* **95**, 7564 (1991).
9. C. Yeretzian, K. Hansen, F. Diederich, R. L. Whetten, *Nature* **359**, 44 (1992).
10. R. D. Beck, P. Weis, G. Brauchle, M. M. Kappes, *J. Chem. Phys.* **100**, 262 (1994).
11. T. W. Ebbesen, H. Hiura, Y. Ochiai, S. Matsui, K. Tanigaki, *Chem. Phys. Lett.* **209**, 83 (1993).
12. Y. Saito, T. Yoshikawa, M. Inagaki, M. Tomita, T. Hayashi, *ibid.* **204**, 277 (1993).
13. S. Seraphin, D. Zhou, J. Jiao, *Carbon* **31**, 1212 (1993).
14. The arcing power supply was an arc welder (Hobart "Porta Tig/Stick," Troy, OH) operating under constant current control, filtered to a residual 3% peak-to-peak sinusoidal ripple at 12 kHz when operating at 100 to 300 A between 15 and 25 V. During operation, the voltage drop across the arc was monitored and via a feedback loop; the vertical separation of the electrodes was adjusted to maintain the desired operating voltage.
15. The five-membered rings (pentagons) that give onion-like particles and closed tube caps their curvature are susceptible to oxidation, in contrast to the perfect graphene tube walls, which are impervious to such oxidative attack. The vastly smaller relative surface area susceptible to etching of long nanotubes compared with their shorter cousins allows the former to outlast the latter under oxidative conditions. This behavior is a manifestation of the one-dimensional nature of carbon nanotubes.
16. R. E. Smalley, *Mater. Sci. Eng.* **B19**, 1 (1993).
17. T. W. Ebbesen, *Annu. Rev. Mater. Sci.* **24**, 235 (1994).
18. Although the conformation with the tube tip open has a higher energy than the closed conformation even in the presence of an electric field, the concentration of negative charge at the tip under such conditions leads to a dramatic increase in the kinetic barrier to closure (L. Luo, P. Nordlander, R. E. Smalley, unpublished results).
19. See, for example, Y. P. Raizer, *Gas Discharge Physics* (Springer-Verlag, Berlin, 1991), chap. 10, and references therein.
20. We estimate the degree of ionization by calculating the carbon cation and neutral densities as follows. The cation density is $n_+ = j_+/v_+$, where j_+ is the cation current density and v_+ is its drift velocity. The cations carry ~20% of the total current [compare with (*19*)], thus $j_+ \simeq 40$ A/cm^2. (We have used here only the area belonging to zone 1.) We estimate the drift velocity to be $\sim 10^4$ cm s^{-1}, yielding a cation density of $\sim 2.5 \times 10^{16}$ cm^{-3}. Because the mass of carbon soot lost from the plasma is only ~10% that of the deposit, we can calculate the carbon neutral density as the flux of atoms lost to the chamber divided by their mean velocity, yielding 2×10^{15} cm^{-3}. Thus, we find an unusually high degree of ionization of ~90%, corresponding to a highly nonequilibrium plasma, contrasting with equilibrium carbon plasmas, which have only a few percent of carbon atoms ionized.
21. A. Yabe, Y. Mori, K. Hijikata, *AIAA J.* **16**, 340 (1978).
22. E. L. Koschmieder, *Bénard Cells and Taylor Vortices* (Cambridge Univ. Press, New York, 1993).
23. We have established that the direction of gravity has no effect on the formation of zones 1 and 2. The same pattern is found on the cathode deposit regardless of whether it is the cathode or the anode that is "on top."
24. If we assume the bulk of the current flows to the tops of the zone 1 columns, the current density there is ~500 A cm^{-2}, which corresponds to 3×10^{20} carbon ions per second per square centimeter, if we assume that 80% of the current is carried by the electrons.
25. See, for example, R. Ruthen, *Sci. Am.* **268**, 130 (January 1993); B. Kaye, *Chaos and Complexity* (VCH Press, New York, 1993); F. Cramer, *Chaos and Order* (VCH Press, New York, 1993), and references therein.
26. This research was supported by the Office of Naval Research, the National Science Foundation, and the Robert A. Welch Foundation, and used equipment designed for study of fullerene-encapsulated catalysts supported by the Department of Energy, Division of Chemical Sciences.

5 August 1994; accepted 7 October 1994

A Phase of Liposomes with Entangled Tubular Vesicles

Shivkumar Chiruvolu, Heidi E. Warriner, Edward Naranjo,
Stefan H. J. Idziak, Joachim O. Rädler, Robert J. Plano,
Joseph A. Zasadzinski,* Cyrus R. Safinya*

An equilibrium phase belonging to the family of bilayer liposomes in ternary mixtures of dimyristoylphosphatidylcholine (DMPC), water, and geraniol (a biological alcohol derived from oil-soluble vitamins that acts as a cosurfactant) has been identified. Electron and optical microscopy reveal the phase, labeled L_{tv}, to be composed of highly entangled tubular vesicles. In situ x-ray diffraction confirms that the tubule walls are multilamellar with the lipids in the chain-melted state. Macroscopic observations show that the L_{tv} phase coexists with the well-known L_4 phase of spherical vesicles and a bulk L_α phase. However, the defining characteristic of the L_{tv} phase is the Weissenberg rod climbing effect under shear, which results from its polymer-like entangled microstructure.

Phospholipid molecules form closed bilayer shells known as liposomes or vesicles when dispersed in water because of the amphiphilic nature of the molecules (*1*). Since their discovery by Bangham *et al.* (*2*), uni- and multilamellar vesicles have received much attention because of their similarities to living cells and their potential for encapsulating and segregating water-soluble materials from a bulk solution (*1*). Vesicles are used extensively as models of adhesion, de-adhesion, and fusion of interacting cells (*1*, *3*) and in fundamental studies of colloidal interactions and stability (*4*, *5*). From a technological viewpoint, vesicles are increasingly used in the cosmetics industries as controlled chemical release agents (such as in formulations of lotions, gels, and creams) (*6*); they continue to be explored for their utility in the food and agricultural industries and are likely to dramatically impact the medical field as drug and gene carriers (*7*).

We report on the discovery of another vesicle phase in room-temperature mixtures of DMPC, water, and geraniol. Geraniol is a branched long-chain biological alcohol, derived from oil-soluble vitamins, that acts as a cosurfactant (Fig. 1). In the DMPC-rich corner of the phase diagram, we observe a lyotropic liquid-crystal multilamellar L_α phase, and in the water-rich corner, an extremely dilute phase of spherical unilamellar vesicles that is similar to the equilibrium vesicle phases (L_4) recently observed in similar systems (*8*–*10*). A phase consisting of entangled multilamellar tubular vesicles, which we have labeled the L_{tv} phase, emerges in the region between the L_α and L_4 phases. The L_{tv} phase responds dramatically to applied flow fields, which strongly indicates that its microstructure is similar to that of a semidi-

---

S. Chiruvolu and E. Naranjo, Materials Research Laboratory and Department of Chemical Engineering, University of California, Santa Barbara, CA 93106, USA.
H. E. Warriner, Materials Research Laboratory, Materials Department, and Physics Department, University of California, Santa Barbara, CA 93106, USA.
S. H. J. Idziak and J. O. Rädler, Materials Research Laboratory and Materials Department, University of California, Santa Barbara, CA 93106, USA.
R. J. Plano, Exxon Research and Engineering Company, Annandale, NJ 08801, USA.
J. A. Zasadzinski, Materials Research Laboratory, Department of Chemical Engineering, and Materials Department, University of California, Santa Barbara, CA 93106, USA.
C. R. Safinya, Materials Research Laboratory, Materials Department, Physics Department, and Biochemistry and Molecular Biology Program, University of California, Santa Barbara, CA 93106, USA.

---

*To whom correspondence should be addressed.